Journal of Nanoscience and Technology 1(1) (2015) 26–31

ISSN: 2455-0191

Contents List available at JACS Directory

Journal of Nanoscience and Technology

journal homepage: www.jacsdirectory.com/jnst

Synthesis and Analysis of Nanocrystalline $Fe_2Mn_2Ni_{0.5}Zn_{1.5}O_9$ at Different Treating Temperatures

S.N. Anitha[1], I. Jayakumari[2,*]

[1]*Department of Physics, D. B. Pamba College, Parumala – 689626, Kerala, India.*
[2]*Centre for Condensed Matter, Department of Physics, CMS College, Kottayam – 686001, Kerala, India.*

ARTICLE DETAILS

Article history:
Received 28 October 2015
Accepted 07 November 2015
Available online 11 November 2015

Keywords:
$Fe_2Mn_2Ni_{0.5}Zn_{1.5}O_9$
SEM
Debye Scherrer
Williamson-Hall
Dislocation Density
EDAX

ABSTRACT

After the discovery of high temperature superconductivity a tremendous change occurred in the crystalline study of nano ceramics. Nanocrystalline ceramics $Fe_2Mn_2Ni_{0.5}Zn_{1.5}O_9$ is prepared from a suitable combination of ferrous oxide, manganese oxide, nickel oxide and zinc oxide. These materials are expected to play an important role in the area of microelectronics, especially for magnetic field sensors, optical detectors, Josephson junctions and interconnects in integrated circuits. In this work, the authors designed a new nano crystalline ceramic type II High-TC superconductor, ferromanganese nickel zinc oxide ($Fe_2Mn_2Ni_{0.5}Zn_{1.5}O_9$). The sample $Fe_2Mn_2Ni_{0.5}Zn_{1.5}O_9$ was prepared by the solid state thermo chemical reaction technique including mixing, milling, calcination and sintering. In order to show the viability of the proposed method, super-conducting powder was prepared in a special furnace. The synthesized material was characterized using XRD, FTIR, SEM and EDAX techniques. Using scanning electron microscopy (SEM) the morphology of the synthesized crystals was scrutinized. The XRD analysis has shown that the synthesized crystal has possessed orthorhombic structure. The X-Ray Diffraction (XRD) analyser is, an indispensable non-destructive tool for structural material characterization and quality control which makes use of the Debye-Scherrer method. The orthorhombic structure of the sample was confirmed by the comparison of XRD results with JCPDS file and applying XPERT-PRO software. X-ray instrumental peak broadening analysis was used to evaluate the crystalline sizes and lattice strain on the peak broadening by the Williamson-Hall Plot method. The Scanning Electron (SEM) micrograph depicts the presence of fine crystallites with assorted morphology which revealed that its particle size is in the nano meter range. And it was confirmed by the calculated value of particle size from Debye Scherrer's formula. From the EDX plot the presence of all the constituents were confirmed. Dislocation density (δ) is also calculated.

1. Introduction

The resistivity of Superconductors drops to zero at sufficiently low temperatures, in contrast with metal conductors whose resistivity decreases as the temperature falls. But it remains finite even at the lowest temperatures [1]. The temperature below which the resistivity of a superconductor goes to zero is known as the critical temperature, Tc and the material becomes superconducting [2]. A superconductor can sustain a current indefinitely with no loss due to resistance below Tc, which is an electrical analog of friction [3, 4]. High-temperature super-conductors (abbreviated high-Tc or HTS) have been observed with transition temperatures as high as 138 K (−135 °C) [5]. In 1986 families of cooperate-perovskite ceramic materials known as high temperature superconductors were discovered, with critical temperatures in excess of 90 Kelvin. As a topic of pure research, these materials represented a new phenomenon not explained by the current theory. In addition, because the superconducting state persists up to more manageable temperatures, past the economically – important boiling point of liquid nitrogen(77 Kelvin), more commercial applications are feasible, especially if materials with even higher critical temperatures could be discovered [6].

Perovskite materials are of great interest because of their very interesting properties, such as magnetic, optical, ferroelectric, and colossal magneto resistance, high-Tc superconductivity, non-volatile memory effects. However, several iron-based compounds are now known to be superconducting at high temperatures [7-9]. Superconductivity can be observed in a wide variety of materials, including simple elements like tin and aluminum, various metallic alloys and some heavily – doped semiconductors. Superconductivity does not occur in noble metals like gold and silver, nor in pure samples of ferromagnetic metals [10]. Since there is a complete expulsion of magnetic flux, superconductors are considered to be perfectly diamagnetic [11, 12]. High-voltage generator can be developed by using HTS inductor and electronic RCL series resonant circuit [13, 14].

Nano crystallinity can improve its electrical properties by strong pinning. In the present work we report the synthesis and analysis of nanocrystalline $Fe_2Mn_2Ni_{0.5}Zn_{1.5}O_9$ superconducting compound by mechano-chemical reaction followed by post - annealing.

In this study the authors describe the synthesis of $Fe_2Mn_2Ni_{0.5}Zn_{1.5}O_9$ nanocrystalline ceramic type II high-TC superconductor material by the solid state thermo chemical reaction technique and it is characterized to show good quality, homogeneity. The results were analyzed by X-Ray Diffraction (XRD), SEM and EDX. X-ray diffraction shows formation of a well-developed nanocrystalline $Fe_2Mn_2Ni_{0.5}Zn_{1.5}O_9$ after annealing of the prepared powder at the temperature range of 500-900 °C for a few hours. The morphology of the synthesized samples was scrutinized using scanning electron microscopy (SEM). EDAX analysis gives the concentration of ions in the prepared compound [15].

The particle size was calculated from XRD details by Debye Scherer formula. The SEM studies revealed that the range of particle of the samples prepared is in hundred-nanometer range. The EDX spectrum of $Fe_2Mn_2Ni_{0.5}Zn_{1.5}O_9$ gave the information on the elemental composition of the material. Using Instrumental Broadening and Williamson-Hall Plot method the particle size and lattice strain of the material were found. Line profile analysis (LPA) refers to the analysis of the shape of the peaks. Dislocation density (δ) an important material property, ie the number of dislocation lines crossing unit area in the sample is counted to give: $\rho D = (n/12)\ m^{-2}$ [16]. This strongly affects the out-of-pile and in-pile properties of materials [17].

*Corresponding Author
Email Address: drjayacmscollege@gmail.com (I. Jayakumari)

Cite this Article as: S.N. Anitha, I. Jayakumari, Synthesis and analysis of nanocrystalline $Fe_2Mn_2Ni_{0.5}Zn_{1.5}O_9$ at different treating temperatures, J. Nanosci. Tech. 1(1) (2015) 26–31.

2. Experimental Methods

The nano-sized ceramic material $Fe_2Mn_2Ni_{0.5}Zn_{1.5}O_9$ has perovskite structure. The chemical formula is ABO_3 for perovskite compounds. They are cubic and the variants are tetragonal and orthorhombic (Fig. (1a)). The most familiar ceramic superconducting materials have perovskite structure [18]. The $Fe_2Mn_2Ni_{0.5}Zn_{1.5}O_9$ was prepared by the thermo chemical solid state reaction technique. This method has the following steps: Weighing the materials, stoichiometric mixing, grinding, calcinations, Addition of binder, pressing into pellets, sintering and finishing. The raw materials ferrous oxide, manganese oxide, nickel oxide, zinc oxide were weighed according to their molecular formula. The pure form of the weighed powders was mixed mechanically by hand mixing in agate mortar for very long time. Using zirconium balls the sample was milled for three weeks to insure homogeneity and quality. Then it was attrition milled for five hours. The sample was then calcined at temperatures 30 °C, 500 °C, and 950 °C to obtain $Fe_2Mn_2Ni_{0.5}Zn_{1.5}O_9$ powder treated at different temperatures. After the furnace is off, on cooling the oxygen was allowed to flow into the furnace at intervals (oxygen annealing). A final furnace temperature of 950 °C was maintained for the intermediate firings. The material becomes much harder to regrind, if it is heated for much higher temperatures.

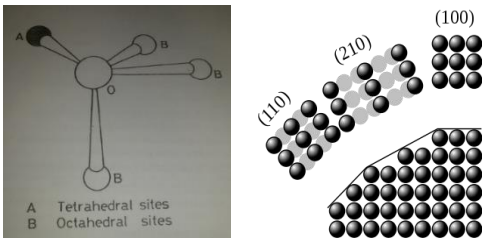

Fig. 1 a) co-ordination of metal ions with oxygen b)Dense Crystalographic planes

The phase evaluation of the sample was analyzed by the X-Ray diffraction spectrum. The powdered sample provides all possible orientations of all possible lattice planes (Fig. 1b). X-ray diffraction spectrum of these materials were taken using Bruker AXS D8 advance diffractometer. The diffractometer with radiations of wavelength 1.541 Å having Nickel filter, equipped with X-ray generator 1140/90/96 having X-ray source KRISTALLOFLXE 780, KF, 4KE with wide angle goniometer PW1710/70 with single pen recorder pm 8203 and channel control PW1390 at 35 kV, 10 mA is used for the purpose. The scanning speed of the specimen is 2 degree/minute. From the XRD results and analyses, it was concluded that this crystal was found to be orthorhombic system. Different methods were used to evaluate the crystallite size of the sample. The crystallite sizes of the materials were calculated from the XRD data by the Debye Scherrer method, W-H analysis and size-strain plot method.

3. Results and Discussion

3.1 Scherrer Method

The crystal morphology and particle size play important roles in the synthesis of nano ceramic materials. So their studies are very important in the research field of ceramics. No crystals are perfect due to their finite size, because a perfect crystal would extend infinitely in all directions. This leads to the broadening of the diffraction peaks. The two main properties extracted from peak width analysis are (a) crystallite size and (b) lattice strain. Crystallite size is a measure of the size of a coherently diffracting domain. Lattice strain is a measure of the distribution of lattice constants arising from crystal imperfections, such as lattice dislocation [19, 20]. The effect of strain, both uniform and non-uniform, on the direction of X-ray reflection is illustrated in Fig. 2.

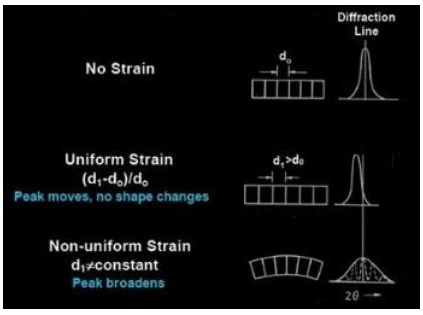

Fig. 2 A portion of an unstrained grain appears in uniform tensile strain and nonuniform strain. According to the figure the uniform strain affect the peak position and the nonuniform strain affect the peak broadening and intensity.

The Bragg width contribution from crystallite size is inversely proportional to the crystallite size [21]. A portion of an unstrained grain appears in panel on the left, where the reflecting planes are equally spaced. If a uniform tensile strain is applied to a grain at right angles to the reflecting planes, their spacing becomes larger than d and the corresponding diffraction line shifts to lower angles but does not otherwise change. The original peak positions and the shifted positions are shown in the Fig. 3. This line shift is the basis of the X-ray method for the measurement. The Bragg width is found to inversely proportional to the crystallite size [22]. W-H analysis is a simplified integral breadth method where size-induced and strain-induced broadening is evaluated by considering the peak width as a function of 2Θ [23].

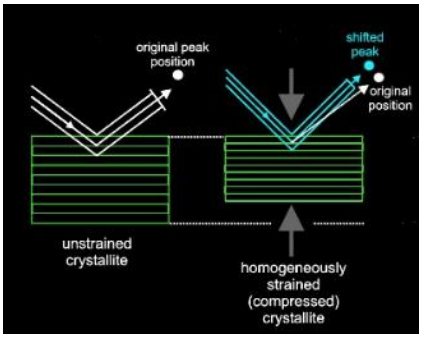

Fig. 3 diffraction on unstrained and compressed crystal planes

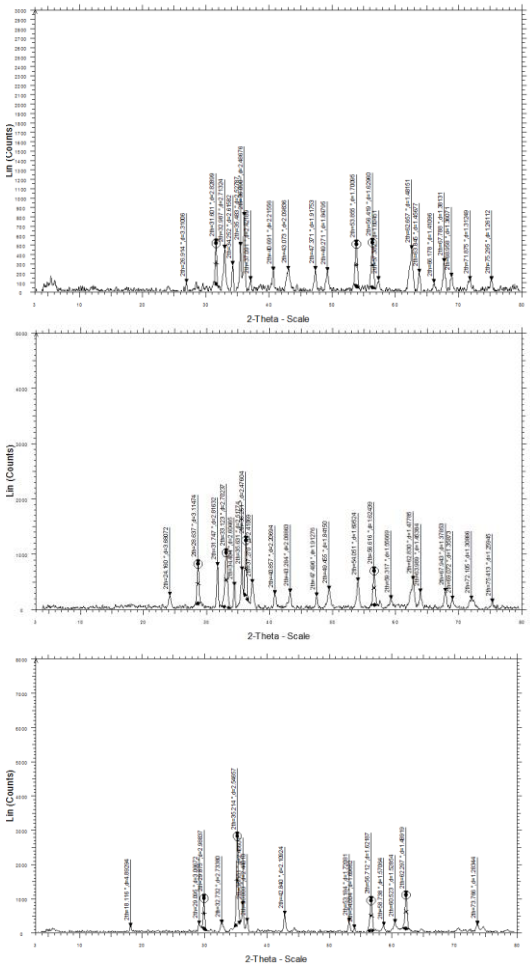

Fig. 4 Shows the XRD diffraction profile of $Fe_2Mn_2Ni_{0.5}Zn_{1.5}O_9$ at temperatures a)30 °C, b)500 °C, c)950 °C

The lines in a powder diffraction pattern are of finite breadth but since the particles were very small, the lines started to broaden than usual. As the crystallite size increases the broadening of the pattern decreases. The particle size of the $Fe_2Mn_2Ni_{0.5}Zn_{1.5}O_9$ was determined by the X-ray line broadening method using the Scherrer equation. The Scherrer equation, is a formula that relates the size of sub-micrometre particles, or crystallites, in a solid to the broadening of a peak in a diffraction pattern. It is named after Paul Scherrer [24, 25]. It is used in the determination of size of

particles of crystals in the form of powder. The Scherrer equation can be written as:

$$D=K\lambda/\beta\cos\theta \quad (1)$$

where D is the mean size of the ordered (crystalline) domains, which may be smaller or equal to the grain size K is a dimensionless shape factor, and the value is taken to be 0.9; λ is the X-ray wavelength; β is the line broadening at half the maximum intensity (FWHM), This quantity is also sometimes denoted as Δ (2θ); θ is the Bragg angle measured. From the results it is concluded that the crystallite size is less than 100 nm. The XRD diffraction profile of $Fe_2Mn_2Ni_{0.5}Zn_{1.5}O_9$ at temperatures 30 °C, 800 °C & 950 °C are given below in Fig. 4. Table 1 gives the hkl indices corresponding to 2θ values. The particle sizes of $Fe_2Mn_2Ni_{0.5}Zn_{1.5}O_9$ calculated at various d/2θ values of different temperatures are shown in the Table 2. Increase in particle size with treating temperatures, diffraction angle theta shifting to right on increase of calcinations temperature of the sample and band width β decreasing on increasing calcinations temperature of the sample $Fe_2Mn_2Ni_{0.5}Zn_{1.5}O_9$ can be visualized in the Fig. 5.

Comparing the XRD data with JCPDS file and applying XPERT-PRO software it is concluded that $Fe_2Mn_2Ni_{0.5}Zn_{1.5}O_9$ have an orthorhombic system, details furnished below.

a ≠ b ≠ c and α = β = γ = 90° - orthorombic system.
a = 8.3716 Å, b = 5.9194°, c = 3.0457 Å. Cell volume =150.9184^{03}

Fig. 4 shows the XRD diffraction profile of $Fe_2Mn_2Ni_{0.5}Zn_{1.5}O_9$ at temperatures (a) 30 °C, (b) 500 °C, (d) 950 °C. Variation of particle size, angle of diffraction shifting to right, the band width (β) decrease with respect to increase in calcination temperature of the sample $Fe_2Mn_2Ni_{0.5}Zn_{1.5}O_9$ are plotted in Fig. 5.

Table 1 The (hkl) indices calculated from the 2θ values of the XRD profile are listed below

2θ in degrees	hkl
29.875	(001)
35.214	(101)
36.803	(200)
42.840	(210)
54.004	(021)
56.712	(121)
62.297	(002)
73.766	(231)

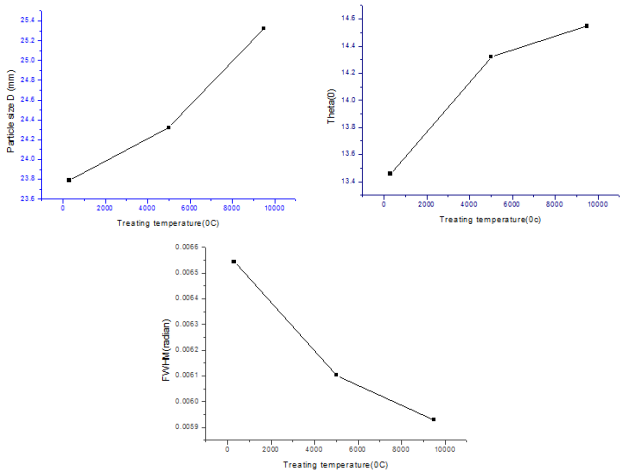

Fig. 5 Shows particle size increase/variation, angle of diffraction shifting to right, β the band width decrease with respect to increase in calcination temperature of the sample - $Fe_2Mn_2Ni_{0.5}Zn_{1.5}O_9$.

The broadening of peak with crystallite size is studied from the XRD data analysis of the sample. Crystals formed may not be perfect due to their finite size. The deviations or disparity from perfect crystallinity leads to the broadening of the diffraction peaks. The two main factors of peak width analysis are the crystallite size and lattice strain. Hence the 2θ peak positions get shifted. The breadth of the Bragg peak is a combination of both instrument and sample dependent effects as

$$\beta^2_{\text{crystallite size}} = \beta^2_{\text{measured}} - \beta^2_{\text{instrumental}} \quad (2)$$

Therefore $D = K\lambda / \beta\cos\theta \Rightarrow \cos\theta\ K\lambda/D(1/\beta)$

3.2 Scherrer Plot Method

The particle size and strain of $Fe_2Mn_2Ni_{0.5}Zn_{1.5}O_9$ changed with the change in treating temperatures. Data of the XRD spectrum of the sample gave evidence of these changes. Due to the change in temperature the peak width and intensity of the peak changed and also 2θ peak position shifted. The crystallite size varies as 1/cosθ and strain varies as tan θ from the peak width. This difference in behavior as a function of 2θ enables one to discriminate between the size and strain effects on peak broadening. The Bragg width contribution from crystallite size varies inversely as the crystallite size [26]. Scherrer Plots were drawn with 1/β on the X-axis and cosθ along the Y-axis at different temperatures as given in the Fig. 6. By linear fitting the data, the crystallite size D was extracted from the slope of the line.

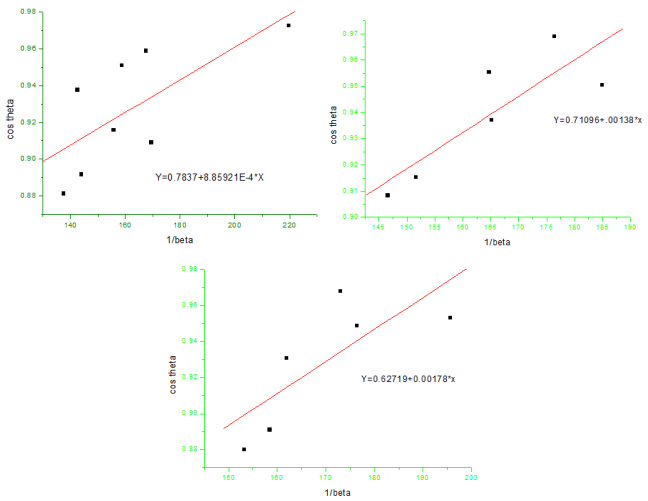

Fig. 6 shows the Scherrer plots of $Fe_2Mn_2Ni_{0.5}Zn_{1.5}O_9$ at different temperatures 30 °C, 500 °C, 950 °C

3.3 Wiliamson- Hall (W-H) Plot method

W-H plot and size-strain plot method is a simplified integral breadth method used to study the changes of the strain and size with respect to the temperature where size-induced and strain-induced broadening are deconvoluted by considering the peak width as a function of 2θ [27]. The peak width derived from crystallite size varies as 1/cos θ whereas strain varies as tanθ. W-H plots emphasised the strain induced plots. This difference in behaviour as a function of 2 θ enables to distinguish between the strain and size effects on peak broadening. The Bragg width contribution from crystallite size is inversely proportional to the crystallite size [28]. Addition of Scherrer formula and the strain induced broadening results in

$$\beta^2_{hkl} = K\lambda/D\cos\theta + 4\varepsilon\tan\theta \text{ ------(3)}$$

where ε represents the strain. W-H plots are drawn with 4sinθ along the X axis βcosθ along the Y axis and as given in Fig. 7. The slope and Y-intersect of the fitted line represent strain and particle size, respectively.

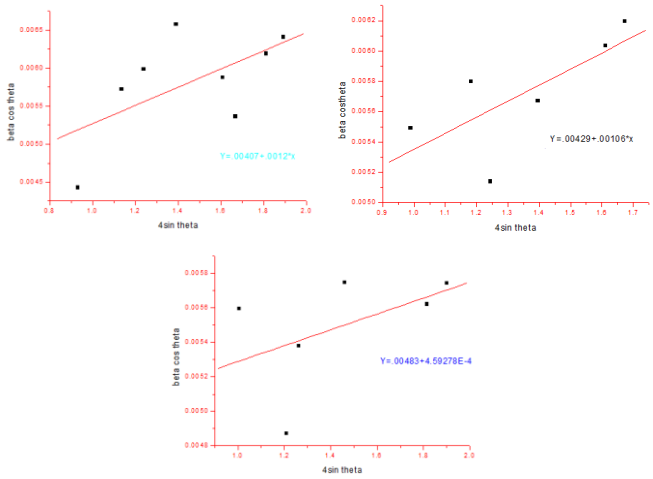

Fig. 7 The W-H plots of $Fe_2Mn_2Ni_{0.5}Zn_{1.5}O_9$ at different temperatures: at a) 30 °C, b) 500 °C, c) 950 °C

3.4 Size-Strain Plot Method

The value of the inter planar spacing between the atoms (d) is calculated using the Bragg's equation,

$$2d\sin\theta = n\lambda \text{ or } d = \frac{\lambda}{2\sin\theta n(n=1)} \quad (4)$$

Wavelength of X ray = 1.5 Å for CuKα.

Due to micro strain contribution the diffracting domains are also isotropic. Size-strain parameters can be obtained from the"Size-Strain Plot" (SSP). Williamson-Hall plot has explained that line broadening was basically isotropic. Here it is assumed that the 'strain profile' is given by Gaussian function and the 'crystallite size' by Lorentzian function [29]. In the Fig. 8 a plot is drawn beween $d^2_{hkl}\,\beta_{hkl}\cos\theta$ and $(d_{hkl}\,\beta_{hkl}\cos\theta)^2$ for all peaks. The crystallite size is calculated from the slope of the linearly fitted data and the root of the Y-intercept gives the strain [28]. The crystallite size D can be measured from the Debye Scherrer formula as $D=0.9\lambda/\beta\cos\theta$

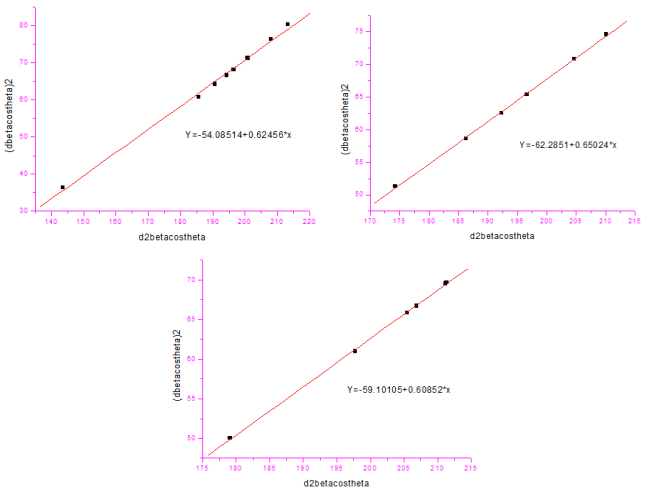

Fig. 8 $(d^2_{hkl}\,\beta_{hkl}\cos\theta)$ versus $(d_{hkl}\,\beta_{hkl}\cos\theta)^2$ plots of $Fe_2Mn_2Ni_{0.5}Zn_{1.5}O_9$ at different temperatures: at a) 30 °C, b) 500 °C , c) 950 °C

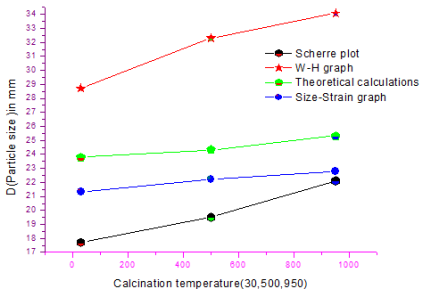

Fig. 9 The crystallite size of the sample $Fe_2Mn_2Ni_{0.5}Zn_{1.5}O_9$ calculated from the different methods.

Table 2 The crystallite size of the sample $Fe_2Mn_2Ni_{0.5}Zn_{1.5}O_9$ calculated from the different methods are listed below

Sample $Fe_2Mn_2Ni_{0.5}Zn_{1.5}O_9$ calcined at different temperatures	XRD values:2θ in degrees		
	At 30 °C	At 500 °C	At 950 °C
Shifting of peak values of XRD with temperature	26.914	28.637	29.095
	32.987	34.404	35.221
	36.090	36.253	36.803
	40.691	40.857	42.840
	47.371	47.496	-
	49.271	49.455	-
	53.851	54.051	54.004
	56.419	56.616	56.714
Average Particle size in nm:			
By theoretical Calculation	23.780	24.320	25.320
From Scherrer plot	17.690	19.500	22.107
From W-H graph	28.706	32.300	34.067
From Size-Strain Plot	21.324	22.200	22.785
Strain from:			
W-H graph	0.00407	0.00429	0.00463
Size-Strain Plot	0.00735	0.007892	0.00780

Comparison of crystalline size of the sample by the different methods of calculation are shown in the Fig. 9. From this it is observed that the crystalline size increases with treating temperatures.

3.5 XRD-Instrumental Broadening

From the observed line broadening we can estimate the average size of the particles. When particle size is less than 100 nm, appreciable broadening in X-ray diffraction lines will occur. Diffraction pattern will show broadening because of particle size and strain. The total broadening of the diffraction peak is due to sample and the instrument. The sample broadening is described by

$$\mathrm{FW(s)} \times \cos\theta = \frac{\mathrm{K} \times \lambda}{\mathrm{size}} + 4 \times \mathrm{strain} \times \sin\theta$$

The total broadening βt equation is described by

$$\beta_t^2 \approx \left\{\frac{0.9\lambda}{\mathrm{Dcos}\theta}\right\}^2 + \{4\varepsilon\tan\theta\}^2 + \beta_0^2$$

Where D is average particle size, ε is strain and βo is instrumental broadening.

3.6 XRD- Dislocation Density

Table 3 Dislocation density (δ), crystallite size and no. of unit cells at the treating temperatures

Transition temperature in °C	Dislocation density	D	n
30	.0001199	23.7875	46.69849
500	.0001089	24.32074	49.90991
950	.0001015	25.3245	56.347739

The dislocation density is a measure of the number of dislocations in a unit volume of a crystalline material [28]. Shift or movement of a dislocation is impeded by other dislocations present in the sample. The properties of the crystal formed are strongly influenced by the defects inside the crystal. Chen and Hendrickson measured and determined dislocation density and hardness of several crystals. A dislocation is an imperfection or crystallographic irregularity or a defect formed within the crystal. As the dislocation density increases the crystal become harder. It has been shown that the dislocation density increases while crystallite size decreases with increasing strain and ultimately these parameters reach saturation values. Above a certain crystallite size limit (~20 nm) the strength of materials increases with decreasing crystallite size. The dislocation density (δ) in the sample (Table 3) has been determined using values of lattice constant, FWHM, θ, and crystallite size. The number of unit cell is calculated from crystallite size and cell volume of the sample [29].

δ = 15βcosθ/4aD, where β, the FWHM measured in radians, θ the diffracting angle, a the cell parameter and D is the crystallite size in nm. The no. of unit cells, $n=\pi\,x(4/3)(D/2)^3\,x1/V$, where V is the cell volume of the sample($V=562.7101^{03}$). Fig. 10 shows the variation of dislocation density (δ) and no. of unit cells with the transition temperatures as shown. The dislocation density decreases with increasing transition temperatures whereas the no of unit cells increases.

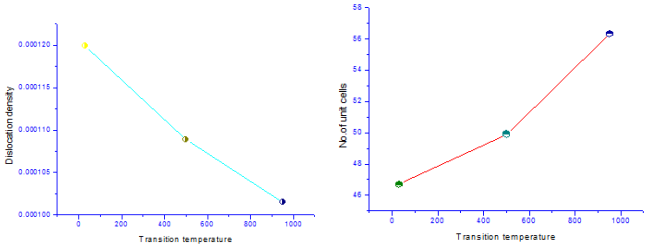

Fig. 10 Variation of dislocation density and no. of unit cells with transition temperatures 30^0, 500^0, and 950^0C of $Fe_2Mn_2Ni_{0.5}Zn_{1.5}O_9$

3.7 SEM Analysis

An idea about the particle size is obtained from the SEM photograph and it helps to arrive on the range of particle size. In SEM analyses the surface of solid objects, producing images of higher resolution than optical microscopy. Fig. 11 shows the surface morphology of the sample $Fe_2Mn_2Ni_{0.5}Zn_{1.5}O_9$. From the crystallite size measurement through SEM revealed that its maximum dimension is always less than 100 nm.

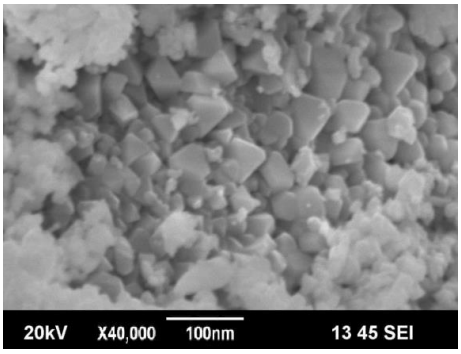

Fig. 11 Surface morphology of $Fe_2Mn_2Ni_{0.5}Zn_{1.5}O_9$

3.8 Energy Dispersed X-Ray Spectrograph (EDX)

Using ISIS Link Oxford Instrument UK. EDAX the sample was recorded. EDAX shows the composition details of the prepared ceramic material (Fig. 12). The above technique is generally associated with Scanning Electron Microscope (SEM). The size of the pulse generated depends on the number electron hole pairs created, which in turn depends on the energy of the incoming X-ray. The detector which is lithium doped silicon is protected by a beryllium window and operated at liquid nitrogen temperatures.

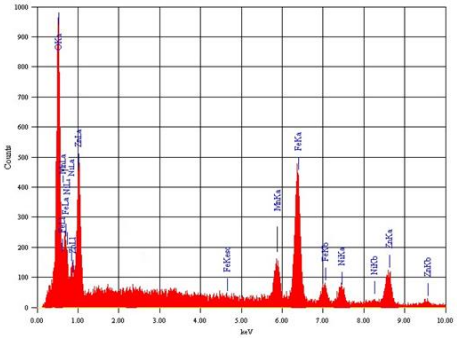

Fig. 12 EDAX spectrum of $Fe_2Mn_2Ni_{0.5}Zn_{1.5}O_9$

From the EDAX spectrum, the dominant peak positions at 6.398, 0.705 keV (FeKα, Lα), 0.637, 5.894 (Mn Lα, Kα), 0.851, 7.471 keV (NiLα, Kα), 1.012, 8.630 keV (Zn Lα, Kα), 0.525 keV (O Kα) correspond quite well to the energy pattern of the corresponding materials (Fe, Mn, Ni, Zn and O) are reported in the EDAX international chart. Percentage composition according to EDAX analysis is shown in Table 4.

Table 4 Percentage composition of prepared sample $Fe_2Mn_2Ni_{0.5}Zn_{1.5}O_9$

Element	(keV)	Mass%
O Kα	0.525	17.7
ZnLα	1.012	20.6
ZnKα	8.630	
NiLα	0.851	7.9
NiKα	7.471	
MnLα	0.637	23.5
MnKα	5.894	
Fe Kα	6.398	30.3
FeLα	0.705	
Total		100

A detailed analysis of the new sample $Fe_2Mn_2Ni_{0.5}Zn_{1.5}O_9$ is successfully done in this work. XRD spectrum gave a clear idea about the maximum intensity peak shifting corresponds to the different treating temperatures. The XRD patterns of $Fe_2Mn_2Ni_{0.5}Zn_{1.5}O_9$ sample obtained for various annealing temperatures are shown in Fig. 4. As the temperature increases, the highest peaks in the XRD spectrums shift from left to right through the 2θ axis (Fig. 5). Line profile analysis of the sample was carefully carried out to analyze the shape of the diffraction peaks. When the material is cooled to room temperature, the amplitude of the atomic vibrations of the material was decreased. But it couldn't arrive at the initial amplitude. The atomic vibration amplitude of the heated material was higher than initial amplitude [30].

The atoms undergo thermal vibration about their mean positions even at the absolute zero of temperature, and the amplitude of this vibration increases as the temperature increases. Increased thermal vibration of the atoms, as the result of an increase in temperature, the unit cell expands, causing changes in d spacing and therefore in the 2θ positions of the diffraction lines. And the intensities of the diffraction lines also decrease.

Crystals with precise periodicities over long distances have sharp and clear diffraction peaks. Crystals with defects (such as impurities, dislocations, planar faults, internal strains, or small precipitates) are less precisely periodic in their atomic arrangements, but they still have distinct diffraction peaks. Their diffraction peaks are broadened, distorted, and weakened, however, and "diffraction line shape analysis" is an important method for studying crystal defects.

Generally, only lattice distortions affect the peak positions whereas structure defects cause a (perhaps also anisotropic) broadening of peaks only.

1. Shift caused due to the stress, strain, dislocation and defects induced since the synthesis parameters.
2. Irradiation effect (Synthesis parameters) might alter the lattice parameters, which may affect the internal properties of the crystal.

Depend upon the internal properties value, peak position shifted towards higher or lower angle.

The shift of diffraction peaks towards higher diffraction angle means crystal lattice is compressed. If the only effect observed is a shift of ALL the Bragg peaks to higher values of the diffraction angle, this means that the lattice parameter is decreasing. Several reasons are possible: the increase in annealing temperature may bring about two changes; 1) increase in the crystallite size, and 2) possible formation of new phases. In the first case, increase in crystallite size modifies the preferences of crystallographic lattice sites, and as a result increase in 2 theta means decrease in lattice constant. In the second case, if there are additional phases, the observed peaks would also change. That means, some existing peaks disappear and some new peaks may appear.

From Fig. 4, the peak broadening in the XRD patterns clearly indicated the nature of formation of the very small nano ceramic material. Shift in peak towards right is an indication of orthorhombic crystal formation tending the sample to attain superconducting state. From the width of the XRD peak, the mean crystallite size is calculated using Debye Scherrer's equation. The values calculated using the Scherrer formula are compared to the values obtained through Scherrer plot, Williamson-Hall plot and the Size-Strain Plot drawn for various temperatures. The disparity or deviations from perfect crystallinity leads to the broadening of the diffraction peaks and hence the 2θ peak positions get shifted. Results agree with the values obtained from different methods.

Table 2 give an idea that confirmed that crystallite size of the material $Fe_2Mn_2Ni_{0.5}Zn_{1.5}O_9$ increases with the increasing treating temperature. The diffraction data proved that the material belongs to orthorhombic system. Heat treatment causes the particles to anneal and form larger grains, which of course indicates that the particles become larger. Hence, the large size of sample at 950 °C is expected. Miller indices, the hkl values calculated from the XRD profile using XPERT – PRO software are listed in the Table 1.

Higher value of dislocation density results in greater hardness. The dislocation density (δ) (Table 3) is determined from the XRD profile. It is clearly confirmed that dislocation density decreases as the treating temperature increases. But the no. of unit cells increase with increase in treating temperatures.

SEM is an experimental proof of the theoretical calculation of crystallite size by Debye Scherrer equation. Fig. 11 shows SEM image of $Fe_2Mn_2Ni_{0.5}Zn_{1.5}O_9$. The SEM photograph revealed that maximum dimensions of the particles are less than 100 nm. Thus SEM visualize the morphology of the particles.

The EDAX analysis indicates that the elements exist in the sample and they agree with the chemical formula of the prepared compound. The EDAX spectrum (Fig. 12) obtained give the confirmation of the elemental composition of the material (Table 4) under investigation.

4. Conclusion

Using the thermo chemical solid state technique nanocrystalline superconducting ceramic $Fe_2Mn_2Ni_{0.5}Zn_{1.5}O_9$ was prepared and is characterized by XRD and SEM analysis. From the XRD line profile analysis the formation of a peroskvite phase at high temperature is observed. The shifting in XRD peak towards right on high annealing temperatures confirms its orthorhombic formation which is a clear indication of its superconducting phase formation. The crystallite size increased as the temperature is increased. The results of broadening analysis by Scherrer plot method, W-H plot method and Size-Strain plot method are in high inter correlation. Characterization with Scanning Electron Microscopy (SEM) revealed that its particle size is in the nanometer and confirmed the calculated value of particle size from Debye Scherrer's formula, W-H and

SSP methods. EDX plot confirmed the presence of all the constituents. Dislocation density (δ) also is calculated. The properties of sample shows that $Fe_2Mn_2Ni_{0.5}Zn_{1.5}O_9$ will definitely have a future in power electronics and microelectronics.

Acknowledgement

The authors are thankful to UGC for the financial Assistance, SAIF, Kochi for providing the instrumental data and to the Principal, CMS College, Kottayam, The principal, D.B.Pampa College, Parumala, Kerala for providing the facilities.

References

[1] J.G. Bendnorz, K.A.Z. Muller, Possible High Tc super conductivity in the Ba-La-Cu-O system, Z. Phys. B. 64 (1986) 189-193.
[2] M.K. Wu, J.R. Ashburn, C.J. Trong, P.H. Hor, L. MengGao, Z.J. Huang, The Effect of Inorganic Nanocrystals on the Properties of High –Temperature Superconductors, Phys. Rev. Lett. 57 (1986) 158-163.
[3] Y.Q. Chu, Super conductivity at 93 K in a new mixed-phase Y-Ba-Cu-O compound system at ambient pressure, Phys. Rev. Lett. 58 (1987) 908-910.
[4] R. Simon, A. Smith, Superconductors conquering technology's new frontier, Plenum Press, New York, 1988.
[5] P.J. Ford, The rise of the superconductors, CRC Press, Florida, 2005.
[6] K. Borgohain, N. Murase, S.J. Mahamuni, Synthesis and properties of Cu_2O quantum particles, J. Appl. Phys. 92 (2002) 1292-1297.
[7] A. Leggett, What DO we know about high Tc?, Nat. Phys. 2(3) (2006) 134-136.
[8] Q. Charles, Choi, Iron exposed as high-temperature superconductor, Scientific American, USA, 2008.
[9] Z. An, Ren, Che, Guang-Can, Dong, Xiao-Li, et al., Superconductivity and phase diagram in iron-based arsenic-oxides ReFeAsO1−δ (Re = rare-earth metal) without fluorine doping, Eurp. Phys. Lett. 83(1) (2008) 17002.
[10] N. Caswell, P.Y. Yu, Physical origin of the anomalous temperature dependence of the 1s yellow exciton luminescence intensity in Cu_2O, Phys. 25 (1982) 5519-5524.
[11] A. Mourachkine, Room-temperature superconductivity, Cambridge International Science Publishing, UK, 2004.
[12] C. Kittel, Introduction to solid state phys., 7th Ed., Wiley, India, 2004.
[13] R.K. Puri, V.K. Babbar, Solid state phys., S Chand and Company Ltd., New Delhi, India, 2009.
[14] A.V. Narlikar, High Temperature Superconductivity, Springer, Berlin, Germany, 2004.
[15] A. Peter Pascal Regis, L. John Berchmans, S. Ignatius Arockiam, Synthesis and characterisation of nano crystalline neodymium nickelate ($NdNiO_3$) powders using low temperature molten salt technique, J. Chem. Sci. 2 (8) (2012) 37-42.
[16] Amelinckx, The direct observation of dislocations, Academic Press, New York, London, 1964.
[17] R.D. Shannon, Revised effective ionic radii and systematic studies of interatomic distances in halides and chalcogenides, Acta. Cryst. 32 (1976) 751–767.
[18] O. Willander, M.Q. Nur, A.B. Israr, F.G. Abou Hamad, E. Desouky , M.A. Salem, I.K. Battisha, Determination of a.c. conductivity of nano-composite perovskite Ba(1–x–y)Sr(x)TiFe(y)O_3 prepared by the sol-gel technique, J. Cry. Pros. Tech. 2 (2012) 1-11.
[19] Amelinckx, The direct observation of dislocations, Academic Press, New York, London, 1965.
[20] F.S. Galasso, Structure, Properties and preparation of perovskite type compounds. pergamon Press, Oxford, COUNTRY, 1969.
[21] K. Ramakanth, Basic of diffraction and its application, I.K. International Publishing House, New Delhi, India, 2007.
[22] V.K. Pecharsky, P.Y. Zavalij, Fundamentals of powder diffraction and structural characterization of materials, Springer, New York, 2003.
[23] C. Suranarayana, M.G. Norton, X-ray diffraction: a practical approach, Plenum Publishing Corporation, New York, , 1998.
[24] A. Patterson, The Scherrer formula for X-Ray particle size determination, Phys. Rev. 56(10) (1939) 978–982.
[25] P. Scherrer, Göttinger Nachrichten Gesell 2 (1918) 98-100.
[26] J. Zhang, Y. Zhang, K.W. Xu, V. Ji, General compliance transformation relation and applications for anisotropic hexagonal metals, Solid State Commun. 139 (2006) 87-91.
[27] A.R. West, Solid state chemistry and its applications, Wiley, New York, 1974.
[28] V.K. Pecharsky, P.Y. Zavalij, Fundamentals of powder diffraction and structural characterization of materials, Springer, Berlin, Germany, 2003.
[29] A. Khorsand Zak, W.H.A. Majid, M.E. Abrishami, Ramin Yousefi, X-ray analysis of ZnO nanoparticles by WilliamsoneHall and sizeestrain plot Methods, Solid State Sci. 13 (2011) 251-256.
[30] R. Hepzi Pramila Devamani, M. Jansi Rani, Synthesis and characterization of lead chromate nanoparticles, Ind. Jour. Sci. Res. 3(4) (2014) 2277-8179.